# Insulating state of ultrathin epitaxial LaNiO₃ thin films detected by hard x-ray photoemission

A. X. Gray,[1,2] A. Janotti,[3] J. Son,[3] J. M. LeBeau,[3] S. Ueda,[4] Y. Yamashita,[4] K. Kobayashi,[4] A. M. Kaiser,[1,2]
R. Sutarto,[5,6] H. Wadati,[5,*] G. A. Sawatzky,[5] C. G. Van de Walle,[3] S. Stemmer,[3] and C. S. Fadley[1,2]

[1]*Department of Physics, University of California, Davis, California 95616, USA*

[2]*Materials Sciences Division, Lawrence Berkeley National Laboratory, Berkeley, California 94720, USA*

[3]*Materials Department, University of California, Santa Barbara, California 93106-5050, USA*

[4]*NIMS Beamline Station at SPring-8, National Institute for Materials Science, Hyogo 679-5148, Japan*

[5]*Department of Physics and Astronomy, University of British Columbia, Vancouver, British Columbia, V6T 1Z1 Canada*

[6]*Canadian Light Source, University of Saskatchewan, Saskatoon, Saskatchewan, S7N0X4, Canada*

In order to understand the influence of strain and film thickness on the electronic structure of thin films of strongly correlated oxides, we have applied hard x-ray photoemission (HXPS) at 6 keV, soft x-ray photoemission (XPS) at 1.5 keV, and transmission electron microscopy to epitaxial LaNiO₃ films deposited on two substrates: LaAlO₃ (compressive strain) and $(LaAlO_3)_{0.3}(Sr_2AlTaO_6)_{0.7}$ (tensile strain). Using inelastic attenuation lengths in LaNiO₃ determined from the HXPS data, we have decomposed valence-band spectra into layer-specific contributions. This decomposition is validated by comparing with the results of first-principles calculations using a hybrid functional. The resultant thin-film LaNiO₃ densities of states exhibit significant differences in spectral weights for the thinnest LaNiO₃ films. A gap opening consistent with a metal-to-insulator transition is observed for the thinnest 2.7 nm LaNiO₃ film on an $(LaAlO_3)_{0.3}(Sr_2AlTaO_6)_{0.7}$ substrate, with a similar gap opening also being observed in complementary soft x-ray photoemission at 1.5 keV for a thinner 1.4 nm film on an LaAlO₃ substrate. A metal-to-insulator transition in very thin nm-scale films of LaNiO₃ is thus suggested as a general phenomenon.

PACS number(s): 79.60.−i, 71.15.Mb, 73.20.At, 82.80.Pv

## I. INTRODUCTION

Determining the composition and electronic structure of strongly correlated perovskite oxides and oxide thin-film heterostructures is critical to understanding their physics and their potential for novel device applications. Much attention has also been devoted recently to theoretical and experimental studies of electron transport in two-dimensional systems, and in particular to the investigation of electronic and magnetic properties of ultrathin "quantum confined" films exhibiting strong electron correlation. As an example of such a system, the rare-earth nickelate LaNiO₃ (LNO) has recently been predicted to exhibit drastic changes in its magnetic and electronic properties as a function of thickness and epitaxial strain.[1–4] Gaining access to such useful properties, including possibly high-temperature superconductivity, has been suggested via heterostructuring.[2] The exact nature and origin of the electronic structure changes associated with such phenomena may in principle be investigated using normal soft x-ray photoelectron spectroscopy (XPS), which provides a direct way of probing core-level and valence-band electronic states. In fact, soft x-ray XPS in the ∼500–1500 eV range has been used to study such systems in the past.[5–8] However, due to the low inelastic mean-free paths (IMFPs) of the photoemitted electrons, these measurements are inherently sensitive to surface conditions, such as roughness and atmospheric contaminant layers. For example, the widely used TPP-2M formula,[9–11] which can be used to estimate the values of IMFPs for most solids, predicts IMFPs of 10–23 Å in LNO for photoelectrons with kinetic energies between 500 and 1500 eV (the standard XPS regime). This degree of surface sensitivity can lead to spectra dominated by surface effects. There is thus a growing interest in taking photoemission

measurements into the hard x-ray regime, with excitation energies ranging from 2 to 15 keV, and resulting IMFPs of 30–150 Å, respectively. With probing depths thus increased by a factor of roughly $E_{kinetic}^{0.75}$ or 3–6, such measurements can become much more bulk sensitive, and surface effects, although still noticeable, will no longer dominate spectra. Here we apply hard x-ray photoemission (HXPS or HAXPES) to LNO thin films grown epitaxially on two different substrates, LaAlO₃ on which the LNO is under compressive strain by −1.32%, and $(LaAlO_3)_{0.3}(Sr_2AlTaO_6)_{0.7}$ on which LNO is under tensile strain by +0.78%, and determine the LNO and substrate valence-band densities of states as a function of film thickness. These data, together with complementary soft x-ray XPS results, reveal a change from metallic to insulating character for the thinnest LNO layers that is consistent with transport measurements on the same samples,[4] and that depends explicitly on the film thickness and epitaxial strain, perhaps assisted by interface-specific electronic structure changes. Calculations of cross-section-weighted densities of states (DOSs) based on density functional theory (DFT) with a hybrid functional confirm the method used to derive the layer-specific densities of states from HXPS and provide additional insights into the results.

## II. EXPERIMENTAL

For the HXPS study, a set of eight epitaxial LNO thin films with varying thickness was fabricated by rf-magnetron sputtering, as described in detail elsewhere.[4] The sample set consisted of coherently strained 2.8 nm, 4.2 nm, 11.1 nm, and 17.6 nm LNO films deposited on an LaAlO₃ (LAO) (001) substrate and 2.7 nm, 4.6 nm, 10.7 nm, and 16.0 nm LNO films deposited on an $(LaAlO_3)_{0.3}(Sr_2AlTaO_6)_{0.7}$ (LSAT) (001)
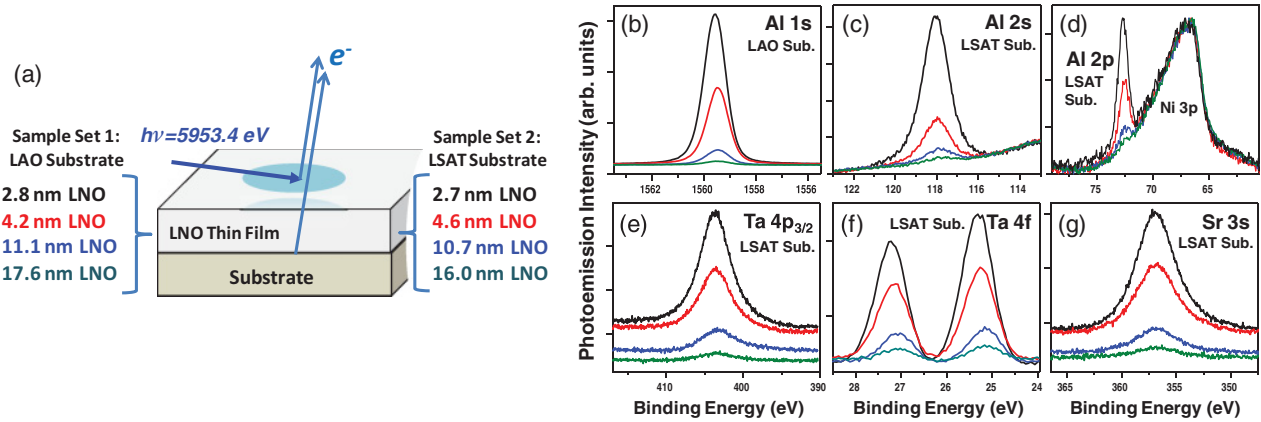
FIG. 1. (Color online) (a) Measured samples and experimental geometry. (b) Photoemission intensity of the Al 1*s* core peak originating from the LAO substrate as the LNO overlayer thickness is increased. Same comparative plots for the Al 2*s* peak (c), Al 2*p* peak (d), and the Ta 4*p*$_{3/2}$ (e), Ta 4*f* (f), and Sr 3*s* (g) core peaks originating from the LSAT substrate. Peaks are normalized to the incident photon flux.

substrate [Fig. 1(a)]. These two substrates subject the LNO to opposite strain, −1.32% compressive for LAO and +0.78% tensile for LSAT. The film thicknesses were determined via cross-section high-resolution scanning transmission electron microscopy (STEM), the LNO/substrate interface was found to be atomically sharp, and the presence of coherent strain through the entire film was verified by x-ray diffraction.

The HXPS measurements were performed at the synchrotron radiation facility SPring-8 in Japan, using the undulator beamline BL15XU, with the photon energy fixed at 5953.4 eV.[12] The photoemitted electrons were analyzed for their kinetic energy by means of a VG Scienta R4000 hemispherical analyzer. Broad survey spectra and individual core spectra from all atoms present, as well as valence-band spectra, were measured, with an overall energy resolution of about 230 meV. The resolution and position of the zero binding energy were determined by frequently measuring the Fermi edge of a Au thin-film standard sample. The exciting radiation was incident on the sample at a grazing angle of 2.0°, as measured from the sample surface. Such an incidence angle yields an x-ray attenuation length of 0.112 $\mu$m for LNO,[13] ensuring that the x-rays penetrate deeply into the bulk; thus the effective attenuation length (EAL) of the photoelectrons is the sole determiner of the probing depth of the experiment. The photoemitted electrons were collected at an angle of 90° as measured from the direction of the incoming x-rays; the electron take-off angle relative to the surface was therefore near normal at 88° and thus yielded maximum bulk sensitivity. All measurements were carried out at ambient temperature, in this case 300 K.

For our very well-defined samples consisting of a thin overlayer film deposited on a substrate, if the film is thin enough, elastic photoelectrons emitted from the substrate can pass through the film and into the detector, contributing to the valence-band spectrum. However, this substrate contribution can be quantified and subtracted, provided that we have precise knowledge of the film thickness and the EAL in the overlayer, which depends on both the IMFP and elastic-scattering effects on the photoelectron trajectories.[11] The photoemission intensity for such a thin-film-on-substrate sample can be

expressed in a standard way as the linear combination of the film- and substrate intensity components:

$$I_{\text{total}} = (1 - e^{-t/\lambda})I_{\text{film}} + e^{-t/\lambda}I_{\text{substrate}},$$

where $t$ is the film thickness and $\lambda$ is the EAL. We make use of this below to first determine the energy-dependent EAL in LNO from core-level intensities, and then to decompose the valence-band (VB) spectra into LNO and substrate components.

To supplement the HXPS results, standard XPS measurements using a monochromatized Al K$\alpha$ source ($hv = 1486.6$ eV) were carried out in the Omicron Multiprobe system located at the Resonant Elastic and Inelastic Soft X-ray Scattering (REIXS) beamline of the Canadian Light Source. With soft x-ray excitation, it was possible to study an even thinner 1.4 nm LNO film on LSAT without noticeable charging effects that were observed for such a film under illumination with a more intense and highly focused hard x-ray beam. Thus, even though XPS will be more surface sensitive, these results are complementary to those of HXPS.

### III. RESULTS AND DISCUSSION

As a first step in the analysis of the HXPS data, we have experimentally determined the EAL of LNO as a function of energy, by measuring the intensities of the core-level peaks originating from the substrate crystal: Al 1*s,* Al 2*s,* and Al 2*p* for both the LAO and LSAT substrates, and Ta 4*p,* Ta 4*f,* and Sr 3*s* for the LSAT substrate. As the thickness of the LNO overlayer increases, the intensity of the core-level peak originating from the substrate decreases [Figs. 1(b)–1(g)]. The peaks were normalized to the incident photon flux, background-subtracted, and fitted using Pseudo-Voigt line shapes (a linear combination of Gaussian and Lorentzian functions). The resulting intensities (areas under the fitted curves) were plotted on a semilog scale versus the STEM-determined LNO overlayer film thicknesses. Since the photoemission intensity of a peak originating from the substrate covered by a uniform overlayer is given by $I_{\text{substrate}} \propto e^{-t/\lambda}$, we have $\log_{10} I_{\text{substrate}} = \log_{10} C - t/2.303\lambda$, where $t$ is
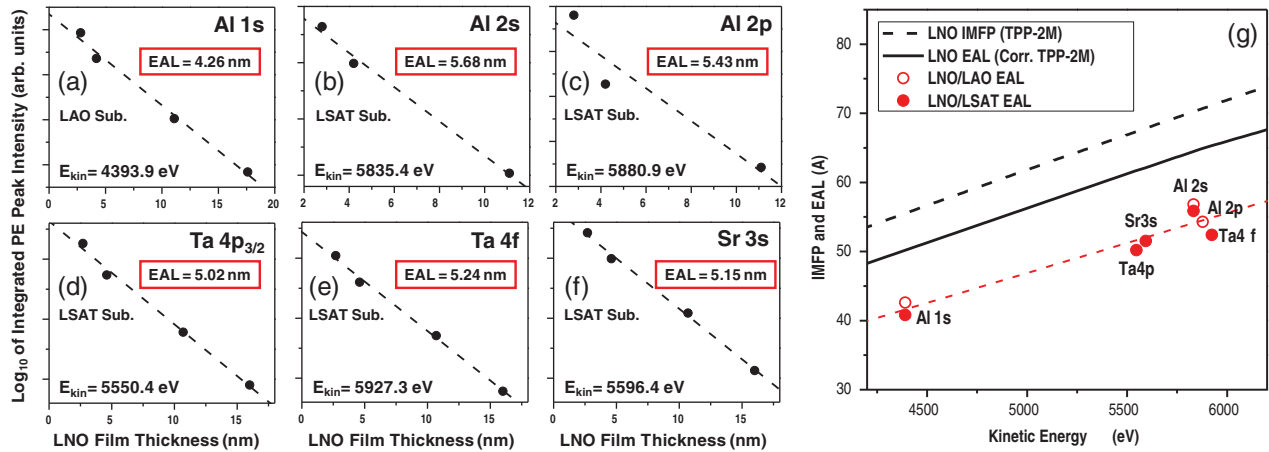
FIG. 2. (Color online) Semilog plot of substrate peak intensities vs LNO overlayer thickness, whose negative slope yields the effective attenuation lengths (EALs) for Al $1s$ photoelectrons with $E_{kin}$ of 4393.9 eV (a), Al $2s$ with $E_{kin}$ of 5835.4 eV (b), Al $2p$ with $E_{kin}$ of 5880.6 eV (c), Ta $4p_{3/2}$ with $E_{kin}$ of 5550.4 eV (d), Ta $4f$ with $E_{kin}$ of 5927.3 eV (e), and Sr $3s$ with $E_{kin} = 5596.4$ eV. In (g), All the EAL values are plotted as a function of $E_{kin}$ and compared to the results obtained using the TPP-2M formula (dashed line)[9,10] and the TPP-2M formula with correction for elastic-scattering effects[11] (solid line).

the overlayer thickness and $\lambda$ is the EAL. Hence, the EAL can be determined from the negative slope of the $\log_{10} I_{substrate}$ versus the overlayer thickness $t$. Figures 2(a)–2(f) depicts such plots and the resultant LNO EALs for six of the eight total substrate core peaks that were measured. The results in general are well described by the simple model expected, but with some systematic deviation for thicknesses in the 4–5 nm range; these deviations are very small for all cases except Al $2p$ for LNO on LSAT, although they do all appear to have the same negative sign. However, for Al $2p$ from LSAT, the deviation is no doubt greater due to having to derive a peak intensity that rides on the Ni $3p$ peak [see Fig. 2(d)]. The systematic negative deviation is most likely due to an uncertainty in the STEM thickness measurement for those particular samples. The values of the EALs are then plotted in Fig. 2(g) versus the kinetic energy of the photoemitted electrons, with excellent agreement to within ~5% being found for peaks arising from the two substrates. For comparison, IMFPs calculated using the TPP-2M formula,[9–11] which represents attenuation via inelastic losses only, are plotted on the same graph (black dashed line). In addition, EALs calculated using the TPP-2M formula but with an additional correction for elastic-scattering effects so as to yield something closer to the EAL[11] are also presented (black solid line). Agreement between the experimental data and the theoretical calculations is excellent, although a systematic 8 Å downwards offset in the experimental EALs is observed. This additional attenuation might be explained by inelastic effects associated with strong resonant core absorption effects, which are not accounted for in the dielectric functions used in the TPP-2M-based calculations.

Having accurately determined the EALs for LNO thin films, we can now analyze the valence-band HXPS spectra and separate the substrate contribution from the thin-film contribution. Extrapolating the experimental EAL plot slightly to the higher kinetic energies of the valence bands, we obtain a best-estimate EAL of 5.5 nm for the electrons originating from the region of 0–10 eV below the Fermi edge. First, we assume that all of the valence-band photoemission intensity for

the thickest LNO sample ($t = t_{max}$) originates from the LNO film, since the thickness is about three times EAL, and the substrate intensity is decreased to $e^{-3} = 0.05$ at the bottom of the thickest films. We can then use the equation above to obtain the substrate contribution to the total photoemission intensity ($I_{substrate}$) for the next thickest LNO sample. Once $I_{substrate}$ is obtained, the following system of linear equations (based on the equation above) can be used to obtain separate photoemission intensities for the valence-band (VB) electrons originating from the LNO film, as well as the LAO substrate or LSAT substrate:

$$I_{exp,t} = (1 - e^{-t/5.5nm})I_{LNO,t} + e^{-t/5.5nm}I_{substrate},$$

$$I_{exp,t=t_{max}} = I_{LNO},$$

where $I_{exp,t}$ is the total normalized experimental VB photoemission intensity for the sample with LNO film thickness $t$, $I_{LNO,t}$ is the isolated film contribution to the total photoemission intensity, and $I_{substrate}$ is the isolated substrate contribution to the total photoemission intensity. These equations can be simply solved to derive the LNO and substrate VB spectra, which should then represent matrix-element-weighted densities of states (DOSs). We have also checked that the neglect of the substrate DOS component for the thickest-LNO samples (17.6 and 16.0 nm) is a valid assumption by modeling the more complex case of inclusion of the signal from the substrate. In fact, the contributions to the overall intensity from the LAO and LSAT substrates are just 4.1% and 5.5%, respectively, and these contributions have been verified numerically not to produce significant changes to the resultant layer-resolved VB spectra. Thus, the thickest-LNO samples (17.6 nm of LNO on LAO and 16.0 nm of LNO on LAO) can indeed be considered as LNO-only. In addition to this, the relative positions of the LNO and substrate spectral-DOS components along the binding-energy scale have been adjusted using as a reference the binding energies of the deep-lying Al $1s$ core levels by about 0.1 eV or less, in order to account for relative shifts the
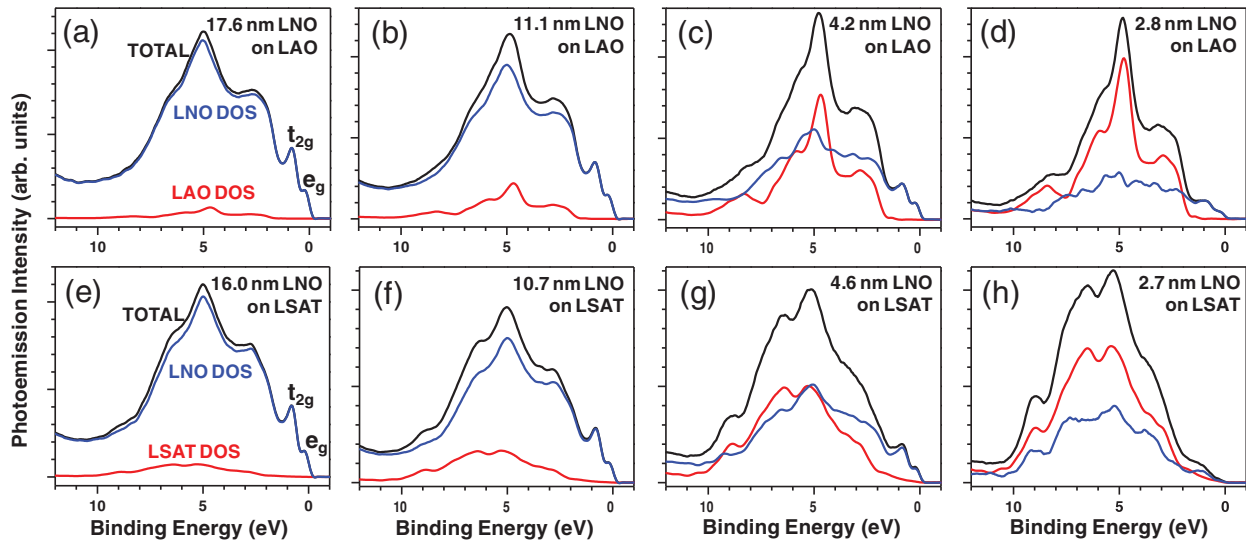
FIG. 3. (Color online) Isolated substrate- and thin-film DOS components for LNO on an LAO substrate (a) 17.6 nm of LNO, (b) 11.1 nm of LNO, (c) 4.2 nm of LNO, and (d) 2.8 nm of LNO. Isolated substrate- and thin-film DOS components for LNO on an LSAT substrate (e) 16.0 nm of LNO, (f) 10.7 nm of LNO, (g) 4.6 nm of LNO, and (h) 2.7 nm of LNO.

two different thicknesses due to band-offset effects between the substrate and the film.[14–16]

The results of the valence-band decomposition are depicted in Figs. 3(a)–3(h). The black curves represent the total photoemission intensity of the LNO/substrate sample, while the red curves and the blue curves represent the isolated intensities of the photoelectrons originating from the substrate and the LNO thin film, respectively. As expected, with decreasing LNO thickness, the contribution of the substrate becomes increasingly prominent (red) and the contribution from the film grows weaker (blue). Both LAO and LSAT exhibit insulating behavior, as is evident from the suppressed photoemission intensity and suggested band gap near the Fermi level. The

LNO film, however, exhibits two prominent features just below the Fermi edge, which, based on prior studies, correspond to Ni $3d\,e_g$ and $t_{2g}$ bands at 0.3 eV and 1.0 eV, respectively.[6,17] We note here that the exact orbital makeup of the feature nearest $E_F$ is the subject of much discussion, and a strong admixture of O $2p$ character can be expected, as well as the possible presence of a Zhang-Rice singlet,[18] that goes beyond a conventional band structure interpretation. Regarding the O $2p$ character, however, the O $2p$ cross section per electron is expected to be only about 1/9 that of Ni $3d$ for our photon energy of 5.9 keV,[19] so its direct effects should be very small in spectra.

In Fig. 4 we now compare the isolated valence-band spectra of LAO [Fig. 4(a)], LSAT [Fig. 4(b)] and LNO
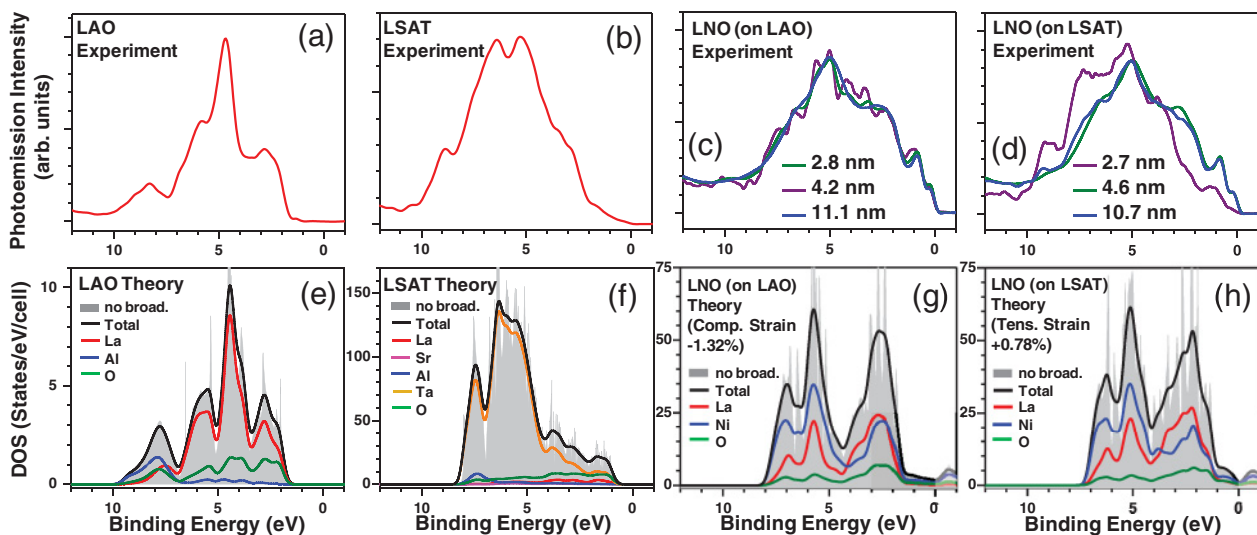


FIG. 4. (Color online) (a) Isolated DOSs for (a) LAO, (b) LSAT, (c) LNO as deposited on an LAO substrate, and (d) LNO as deposited on an LSAT substrate are compared to their respective theoretical spectra (e)–(h) obtained using first-principles hybrid-functional calculations. Experimental LNO spectra are normalized so that the total areas under the curves are equal. Theoretical spectra for LAO and LSAT are shifted in binding energy such that the valence-band maxima for theory and experiment are aligned.

[Figs. 4(c)–4(d)] to photoelectric cross-section-weighted total DOSs obtained using first-principles hybrid DFT calculations [Figs. 4(e)–4(h)]. Individual element-projected DOSs, also weighted by cross section, are also shown. The DOS calculations are based on the HSE hybrid functional and the projector augmented wave potentials as implemented in the VASP code.[20–23] The LAO was simulated using a five-atom primitive cell of the cubic perovskite crystal structure, with a calculated lattice constant $a = 3.78$ Å. LSAT, which constitutes a random alloy with composition $(LaAlO_3)_{0.3}$-$(SrAl_{0.5}Ta_{0.5}O_3)_{0.7}$, was modeled using a 40-atom cubic supercell with composition of $2(LaAlO_3)$-$6(SrAl_{0.5}Ta_{0.5}O_3)$, i.e., $(LaAlO_3)_{0.25}$-$(SrAl_{0.5}Ta_{0.5}O_6)_{0.75}$, and calculated (cubic) lattice constant of 3.89 Å. The LNO was simulated using a tetragonal supercell containing 20 atoms, in which the in-plane lattice constant was fixed to that of LAO or LSAT, and the out-of-plane lattice constant was allowed to relax. All calculations were thus for three-dimensionally periodic structures and are thus most directly comparable to the curves for LAO and LSAT in Figs. 4(a)–4(b), and those for the thickest films of LNO in Figs. 4(c)–4(d). The calculated DOSs were scaled by taking into account the free-atom differential cross-section parameters tabulated in Ref. 19 and including corrections for the effects of experimental geometry and nondipole effects.[24,25] That is, if the differential cross section for a given valence atomic orbital is $\frac{d\sigma_j}{d\Omega}$, and the projected density of states for this orbital at energy $E$ is $\rho_j(E)$, then the predicted curve is given by $I(E) = \sum_j \frac{d\sigma_j}{d\Omega} \rho_j(E)$. The filled areas in Figs. 4(e)–4(h) depict the raw calculation results, which have considerable irresolvable fine structure; the solid curves are obtained by a Gaussian smoothing of 0.23 eV, which simulates smearing due to the effects of total experimental resolution.

The weighted DOS for the LAO substrate is in excellent agreement with the experimental data, with all features being predicted as to position and approximate relative intensity. That of LSAT shows good agreement as to the number and approximate positions of features, although the overall bandwidth is too narrow. This is not surprising, considering that LSAT was modeled using an ordered, rather than a random, structure, with a composition that is actually slightly different from the experimental one. These results thus confirm our basic method for decomposing the VB spectra into layer-resolved components.

Figures 4(c) and 4(d) depict experimental densities of states of LNO films deposited on the two substrates for three different LNO thickness values. For the LAO substrate [Fig. 4(c)], all three films exhibit similar behavior, apart from some minor fluctuations around a common form, which are likely to arise due to noise amplification during the valence-spectra components subtraction for the thinner films. The most significant differences are observed for the experimental DOSs obtained for LNO films deposited on the LSAT substrate [Fig. 4(d)]. The two thicker films exhibit similar behavior. But the DOS for the thinnest film (2.7 nm) exhibits a significant shift in the spectral weight toward higher binding energy and a strong suppression of the DOS just below the Fermi level, which is the region dominated by the Ni $3d$ $e_g$ and $t_{2g}$ bands, and perhaps other more complex O-derived features, as discussed above. This result is consistent with the recent
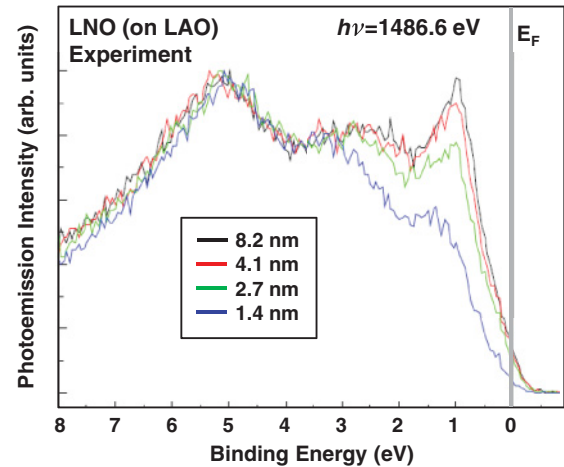


FIG. 5. (Color online) Soft x-ray XPS valence-band spectra of ultrathin LNO films on LAO substrate were collected at normal emission. The various thicknesses of the LNO films were indicated in the legend. The thinnest (1.4 nm) film shows a noticeable suppression of the spectral weight near the Fermi level.

observation of a metal-to-insulator transition in the LNO thin film by means of electron transport measurements.[4]

Complementary XPS measurements with 1486.6 eV excitation on a similar set of LAO-substrate samples have in fact observed a similar metal-to-insulator transition for an even thinner LNO film (1.4 nm), with the raw spectra from these results being shown in Fig. 5. Although one can argue that surface effects might more strongly influence these XPS results, the fact that only for the 1.4 nm film is there significant evidence of the opening of a gap, even though similar surface alterations might be expected for the 2.7 nm or thicker films as well, leads us to conclude that these data support the same sort of conclusion as our more deeply sensing HXPS study with layer-specific decomposition of DOSs, which could not be applied to this thin an LNO layer on LAO due to strong charging effects observed. Thus, we conclude that on both substrates, with either compressive or tensile strain, HXPS and XPS combine to show that very thin LNO films tend to become insulating. It is important to point out that the fact that a band gap appears to be opening shows that the transition to the insulating state is not entirely driven by disorder (Anderson localization) but is rather more like a Mott transition.

The calculated cross-section-weighted DOSs for ideally strained LNO on LAO and LSAT substrates, as shown in Figs. 4(g)–4(h) show more differences from the experimental results. The calculated DOSs show a dip near the Fermi level, which resembles the discontinuity in the derivative of the band dispersion characteristic of the description of metals by Hartree-Fock theory,[26] but they do not clearly indicate the formation of a gap with strain for the bulk system modeled. For the thicker films, the presence of the features ascribed to Ni $3d e_g$ and $t_{2g}$ states are more pronounced in experiment than in theory. There is also a dip in the calculated DOSs at around 4.0–4.5 eV that is not present in experiment. We attribute these differences to deficiencies of DFT, even with an advanced hybrid functional, to describe the band structure of strongly correlated metals, especially near the Fermi level. Also, it may be necessary to include the precise thin-film

geometry for LNO, instead of the bulk-based calculation model used here; we are thus neglecting interface effects that could be important for describing thinner films. Details of the hybrid functional results and a comparison of them with conventional DFT functional are offered in a Supplemental Material section,[27] where total, element-, and orbital-projected results are presented.

suggests a metal-to-insulator transition, as recently observed in similar thin LNO films via electron transport measurements.[4] Complementary soft x-ray XPS measurements for LNO on LAO with thickness down to 1.4 nm permit concluding that very thin LNO films undergo such a transition under either compressive or tensile strain, although interface-specific effects unique to each substrate may also be involved.

## IV. CONCLUSIONS

In summary, we have experimentally determined individual-layer DOSs for thin films of LNO on two different substrates (LAO and LSAT) by first deriving accurate experimental values of the effective attenuation lengths (EALs) in LNO from core-level HXPS spectra from a series of LNO thin-film samples with varying overlayer thicknesses. The resultant EAL values were then used to decompose the valence-band HXPS spectra into DOS contributions from thin film and substrate, and this procedure validated by comparing to substrate theory. The resultant thin-film LNO DOSs were compared for various thicknesses and substrate materials. Significant differences in the spectral weights are observed for the thinnest 2.4 nm epitaxial film on the LSAT substrate. Strong suppression of the DOS just below the Fermi level

*Present address: Department of Applied Physics and Quantum-Phase Electronics Center (QPEC), University of Tokyo, Bunkyo-ku, Tokyo 113-0032, Japan.

[1] J. B. Torrance, P. Lacorre, A. I. Nazzal, E. J. Ansaldo, and C. Niedermayer, Phys. Rev. B **45**, 8209 (1992).

[2] P. Hansmann, X. Yang, A. Toschi, G. Khaliullin, O. K. Andersen, and K. Held, Phys. Rev. Lett. **103**, 016401 (2009).

[3] R. Scherwitzl, P. Zubko, C. Lichtensteiger, and J.-M. Triscone, Appl. Phys. Lett. **95**, 222114 (2009).

[4] J. Son, P. Moetakef, J. M. LeBeau, D. Ouellette, L. Balents, S. J. Allen, and S. Stemmer, Appl. Phys. Lett. **96**, 062114 (2010).

[5] M. Takizawa *et al.*, Phys. Rev. Lett. **97**, 057601 (2006).

[6] K. Horiba, R. Eguchi, M. Taguchi, A. Chainani, A. Kikkawa, Y. Senba, H. Ohashi, and S. Shin, Phys. Rev. B **76**, 155104 (2007).

[7] R. Eguchi, A. Chainani, M. Taguchi, M. Matsunami, Y. Ishida, K. Horiba, Y. Senba, H. Ohashi, and S. Shin, Phys. Rev. B **79**, 115122 (2009).

[8] H. Wadati, A. Maniwa, A. Chikamatsu, H. Kumigashira, M. Oshima, T. Mizokawa, A. Fujimori, and G. A. Sawatzky, Phys. Rev. B **80**, 125107 (2009).

[9] C. J. Powell, A. Jablonski, I. S. Tilinin, S. Tanuma, and D. R. Penn, J. Electron Spectrosc. Relat. Phenom. **98**, 1 (1999).

[10] S. Tanuma, C. J. Powell, and D. R. Penn, Surf. Interface Anal. **43**, 689 (2011).

[11] A. Jablonski and C. J. Powell, J. Vac. Sci. Technol. A **27**, 253 (2009).

[12] K. Kobayashi *et al.*, Appl. Phys. Lett. **83**, 1005 (2003).

[13] B. L. Henke, E. M. Gullikson, and J. C. Davis, At. Data Nucl. Data Tables **54**, 181 (1993).

[14] R. Pentcheva and W. E. Pickett, Phys. Rev. B **78**, 205106 (2008).

[15] Z. S. Popović, S. Satpathy, and R. M. Martin, Phys. Rev. Lett. **101**, 256801 (2008).

[16] R. Pentcheva and W. E. Pickett, J. Phys.: Condens. Matter **22**, 043001 (2010).

[17] J. P. Kemp and P. A. Cox, Solid State Commun. **75**, 731 (1990).

[18] L. H. Tjeng *et al.*, Phys. Rev. Lett. **78**, 1126 (1997).

[19] J. H. Scofield, Tech. Rep., LLNL Report No. UCRL-51326 (1973).

[20] P. Hohenberg and W. Kohn, Phys. Rev. **136**, B864 (1964).

[21] W. Kohn and L. J. Sham, Phys. Rev. **140**, A1133 (1965).

[22] J. Heyd, G. E. Scuseria, and M. Ernzerhof, J. Chem. Phys. **118**, 8207 (2003); **124**, 219906 (2006).

[23] G. Kresse and J. Furthmüller, Phys. Rev. B **54**, 11169 (1996).

[24] M. B. Trzhaskovskaya, V. I. Nefedov, and V. G. Yarzhemsky, At. Data Nucl. Data Tables **77**, 97 (2001).

[25] M. B. Trzhaskovskaya, V. K. Nikulin, V. I. Nefedov, and V. G. Yarzhemsky, At. Data Nucl. Data Tables **92**, 245 (2006).

[26] N. W. Ashcroft and N. D. Mermin, in *Solid State Physics* (Saunders College Publishing, San Diego, 1976).

[27] See Supplemental Material at http://link.aps.org/supplemental/10.1103/PhysRevB.84.075104 for hybrid functional and DFT functional calculations.